British Journal of Pharmacology (2008) 153, 1474–1484
 0007–1188/08 $30.00
www.brjpharmacol.org

RESEARCH PAPER

Influence of the M3–M4 intracellular domain upon nicotinic acetylcholine receptor assembly, targeting and function

S Kracun, PC Harkness, AJ Gibb and NS Millar

Department of Pharmacology, University College London, London, UK

Background and purpose: The aim of this study was to investigate the influence of the intracellular domain of nicotinic acetylcholine receptor (nAChR) subunits upon receptor assembly, targeting and functional properties.
Experimental approach: Because most nAChR subunits form functional receptors only as heteromeric complexes, it can be difficult to examine the influence of individual subunits or subunit domains in isolation. A series of subunit chimaeras was constructed which contain the intracellular loop region (located between the M3 and M4 transmembrane domains) from nAChR subunits α1–α10 or β1–β4. All of these chimaeras contain common extracellular and transmembrane domains (from the nAChR α7 subunit and the 5-hydroxytryptamine receptor 5-HT_{3A} subunit, respectively), thereby facilitating both homomeric receptor assembly and detection with radiolabelled or fluorescent α-bungarotoxin.
Key results: The nAChR M3–M4 intracellular loop domain had no significant effect upon levels of total subunit protein detected in transfected cells but had a significant influence upon levels of both cell surface and intracellular assembled receptors. Comparisons of functional properties revealed a significant influence of the intracellular loop domain upon both single-channel conductance and receptor desensitization. In addition, studies conducted in polarized epithelial cells demonstrate that the nAChR loop can influence receptor targeting, resulting in either polarized (apical) or non-polarized distribution.
Conclusions and implications: Evidence has been obtained which demonstrates that the large intracellular loop domain of nAChR subunits can exert a profound influence upon receptor assembly, targeting and ion channel properties.
British Journal of Pharmacology (2008) **153,** 1474–1484; doi:10.1038/sj.bjp.0707676; published online 21 January 2008

Keywords: nicotinic acetylcholine receptor; receptor assembly; receptor targeting; single-channel conductance

Abbreviations: 5-HT_3R, 5-hydroxytryptamine receptor type 3; αBTX, α-bungarotoxin; DMPP, 1,1-dimethyl-4-phenylpiperazinium iodide; FLIPR, fluorometric imaging plate reader; HBSS, Hanks' buffered saline solution; nAChR, nicotinic acetylcholine receptor; MLA, methyllycaconitine

Introduction

Nicotinic acetylcholine receptors (nAChRs) are oligomeric neurotransmitter-gated ion channels in which five subunits co-assemble to form a central ion channel pore. Nicotinic receptors are prototype members of the 'Cys-loop' family of ligand-gated ion channels, a family that also includes receptors for 5-HT_3 receptors, $GABA_A$ receptors and glycine receptors (Lester *et al.*, 2004; Millar, 2006). In vertebrates, 17 distinct nAChR subunits (α1–α10, β1–β4, γ, δ and ε) have been identified, which can co-assemble to generate a diverse family of nAChRs (Le Novère and Changeux, 1995; Millar, 2003; Alexander *et al.*, 2007).

Correspondence: Professor NS Millar, Department of Pharmacology, University College London, Gower Street, London WC1E 6BT, UK.
E-mail: n.millar@ucl.ac.uk
Received 5 September 2007; revised 9 November 2007; accepted 21 November 2007; published online 21 January 2008

Individual nAChR subunits adopt a complex membrane topology, comprising a large extracellular N-terminal agonist-binding domain and four α-helical transmembrane domains (M1–M4). Previous studies have indicated that the large intracellular domain (between M3 and M4) of nAChRs is important for interaction with intracellular proteins (Jeanclos *et al.*, 2001; Huebsch and Maimone, 2003), receptor targeting (Williams *et al.*, 1998) and ion channel properties (Kelley *et al.*, 2003; Hales *et al.*, 2006; Gee *et al.*, 2007). The aim of the present study is to undertake a detailed comparison of intracellular domains from different nAChR subunits. This has been achieved by the construction of a series of subunit chimaeras containing a common extracellular domain (from the nAChR α7 subunit) and transmembrane domains (from the 5-HT_{3A} subunit), but with different nAChR intracellular loop domains.

Most nAChR subunits form only heteromeric complexes in which an α-subunit must co-assemble with at least one other type of subunit to generate a functional receptor. A well-characterized example is the nAChR expressed at the adult neuromuscular junction, which is assembled from four different subunits (two copies of the α1 subunit co-assembled with a single copy of each of the β1, δ and ε subunits). Similarly, most nAChRs expressed in the nervous system (neuronal nAChRs) are heteromeric complexes (Le Novère and Changeux, 1995; Millar, 2003; Alexander *et al*., 2007). There are a few examples of nAChR subunits, which are able to generate functional homomeric receptors, notably α7, α8 and α9 (Couturier *et al*., 1990; Elgoyhen *et al*., 1994; Gerzanich *et al*., 1994). However, in each case, there is evidence that these subunits are also able to form heteromeric complexes in at least some species (Keyser *et al*., 1993; Gotti *et al*., 1994; Elgoyhen *et al*., 2001).

As a consequence of the propensity of nAChR subunits to assemble into heteromeric complexes, it can be difficult to examine the influence of individual subunits (or individual subunit domains) in isolation. To examine the influence of intracellular loop domains from individual subunits independently, a series of subunit chimaeras has been constructed and characterized. Chimaeras have been constructed containing the intracellular (M3–M4) loop domain from all vertebrate neuronal nAChR subunits (α2–α10 and β2–β4) and from the muscle nAChR α1 and β1 subunits. The starting point for constructing this series of 'loop chimaeras' was a previously described nAChR/5-HT_3R subunit chimaera containing the extracellular, agonist/antagonist-binding domain of the nAChR α7 subunit and the transmembrane domains of the 5-HT_{3A} subunit, which, like the native α7 and 5-HT_{3A} subunits, is able to form functional homomeric ion channels (Eiselé *et al*., 1993; Cooper and Millar, 1998). In contrast to the considerable problems that have been encountered in expression of the nAChR α7 subunit in several mammalian cell lines (Cooper and Millar, 1997; Kassner and Berg, 1997; Rangwala *et al*., 1997), a major advantage of the α7/5-HT_{3A} chimaera is that it forms a functional ion channel very much more efficiently (Cooper and Millar, 1998). Retention of the α7 extracellular domain in the loop chimaeras permits detection of all subunit chimaeras with the α7 antagonist α-bungarotoxin (αBTX), either in radiolabelled form ([^{125}I]αBTX) or conjugated to a fluorescent tag (Alexa-488 αBTX).

By constructing an extensive series of related subunit chimaeras containing a variety of different intracellular loop domains, it has been possible to examine the influence of this domain upon aspects of receptor assembly, targeting and function. This was achieved using a variety of experimental techniques, including radioligand binding, immunoprecipitation, fluorescence confocal microscopy and whole-cell electrophysiology.

Materials and methods

Construction of subunit chimaeras

The construction of a chimaera ($\alpha7^{V201-5HT3A}$) containing the rat nAChR α7 subunit extracellular domain and the mouse 5-HT_{3A} subunit transmembrane and intracellular domains has been described previously (Cooper and Millar, 1997), as has been described for a related chimaera ($\alpha7^{4TM-5HT3A}$) in which the 5-HT_{3A} intracellular loop domain has been replaced with the equivalent region of the α7 subunit (Gee *et al*., 2007). Unique restriction enzyme sites (*Not*I and *Bst*Z17I) were introduced at the N- and C-terminal ends of the large M3–M4 intracellular loop domain of $\alpha7^{4TM-5HT3A}$ by use of the QuikChange site-directed mutagenesis system (Stratagene, Amsterdam, The Netherlands) to create $\alpha7^{4TM-5HT3A(Not/Bst)}$. In the original $\alpha7^{4TM-5HT3A}$ construct, the amino-acid sequence at the M3 end of the M3–M4 loop is QDLQRP/MPKWTR (where '/' indicates the junction between 5-HT_{3A} and α7 sequence). The first Met of the α7 sequence corresponds to position 327 in the rat α7 sequence (numbered according to Figure 1 of Séguéla *et al*., 1993). Introduction of the *Not*I site altered the first amino acid of the α7 sequence from Met to Leu in $\alpha7^{4TM-5HT3A(Not/Bst)}$. The amino-acid sequence at the M4 end of the M3–M4 loop in $\alpha7^{4TM-5HT3A}$ is KFAACV/LDRLLF (where '/' indicates the junction between α7 and 5-HT_{3A} sequence). The final Val of the α7 sequence corresponds to position 466 in the rat α7 sequence (numbered according to Figure 1 of Séguéla *et al*., 1993). Introduction of the *Bst*Z17I site altered the last amino acid of the α7 sequence from Val to Ile in $\alpha7^{4TM-5HT3A(Not/Bst)}$. To generate a series of 'loop chimaeras', the M3–M4 intracellular loop domain was amplified by PCR from nAChR subunit cDNA constructs with primers designed to introduce *Not*I and *Bst*Z17I sites. Fragments were amplified from rat cDNA clones, with the exception of α8 which has not been identified in mammalian species and was amplified from chicken cDNA. After digestion with *Not*I and *Bst*Z17I, PCR fragments were ligated into the *Not*I and *Bst*Z17I sites of $\alpha7^{4TM-5HT3A(Not/Bst)}$. All plasmid constructs (in the mammalian expression vector pZeoSV2+; Stratagene) were verified by nucleotide sequencing. The series of nAChR subunit M3–M4 intracellular loop domain chimaeras will be referred to as $\alpha7/5\text{-}HT_{3A}{}^{\alpha1\text{-loop}}$ (etc.) or, more simply, as 'α1 loop' chimaera (etc.).

Heterologous expression in tsA201 and MDCK cells

Human embryonic kidney (tsA201) cells were cultured in Dulbecco's modified Eagle's medium containing 2 mM L-Glutamax (Invitrogen-Gibco, Paisley, UK) and 10% heat-inactivated FCS (fetal calf serum) (Sigma-Aldrich, Poole, UK) at 37 °C in an atmosphere of 5% CO_2. Cells were transfected using the Effectene transfection kit (Qiagen, Crawley, UK) according to the manufacturer's instructions. Madin–Darby canine kidney (MDCK) cells were transfected using a modified Effectene protocol, in which a higher ratio of transfection mixture to medium (2:1) was used. MDCK cells were maintained in a humidified incubator at 37 °C with 5% CO_2. Cells were trypsinized 12–18 h after transfection and re-seeded on Costar Transwell Clear Permeable Supports (0.4 μm pore size, polyester membrane; Qiagen) and re-incubated, as above, to induce polarization. Forty-eight hours after transfection, MDCK cells were processed for immunocytochemistry.

Immunocytochemistry

Madin–Darby canine kidney cells were washed three times with phosphate-buffered saline until loose cells and cell debris were removed from the cell monolayer. The polyester membrane was carefully excised from the surrounding support using a scalpel, marked for orientation and fixed in 3% paraformaldehyde for 15–30 min. The membranes were then washed five times in Hanks' buffered saline solution (HBSS), permeabilized with 1% Triton/HBSS, for 15–30 min and blocked for 30 min in blocking solution containing 2% BSA/5% FCS/1% Triton/HBSS. Cells were incubated for 2 h at room temperature or overnight at 4 °C in blocking solution containing Alexa-488 αBTX (Invitrogen-Gibco) and DECMA-1 rat monoclonal antibody against E-cadherin, (U3254; Sigma-Aldrich). Cells were washed five times in HBSS, re-blocked for 30 min and then incubated for 1 h at room temperature or overnight at 4 °C in blocking solution containing rhodamine-conjugated goat anti-rat IgG secondary antibody (31680; Pierce, Cramlington, UK). Cells were washed five times in HBSS, once in water and then mounted under glass in Fluosave mounting fluid, with the apical cell surface facing upwards. Confocal images were obtained with a Zeiss LSM 510 Meta confocal microscope and LSM acquisition software. Images were processed using Volocity image analysis software (Improvision, Coventry, UK).

Radioligand binding

Radioligands [^{125}I]αBTX (specific activity 7.4 TBq mmol^{-1}) and [^{3}H]methyllycaconitine (MLA; specific activity 2.2 TBq mmol^{-1}) were purchased from GE Healthcare (Little Chalfont, UK) and Perkin Elmer (Seer Green, UK), respectively. For studies with both intact and disrupted cells, cell monolayers were rinsed and collected in HBSS and pelleted by gentle centrifugation. Cell membranes were prepared by freeze/thawing of cell pellets and were resuspended in phosphate buffer containing protease inhibitors (with final concentrations of 1 μg ml^{-1} pepstatin, 2 μg ml^{-1} leupeptin, 2 μg ml^{-1} aprotinin), transferred to 5 ml polystyrene assay tubes and incubated with radioligand (10 nM [^{125}I]αBTX or 10 nM [^{3}H]MLA) for 2 h, shaking, on ice. In the case of αBTX binding, 1% BSA was added to the assay. Nonspecific binding was determined with 1 mM nicotine and 1 mM carbachol. For cell-surface [^{125}I]αBTX binding, cells were prepared as above except, after pelleting, cells were resuspended by gentle agitation and pipetting, and assayed in HBSS (containing protease inhibitors, as above) at room temperature. [^{125}I]αBTX and [^{3}H]MLA-labelled samples were harvested using a Brandel cell harvester (Model M36; Semat, St Albans, UK) onto Whatman GF/A and Whatman GF/B filters (respectively) and pre-soaked for at least 1 h in 0.5% w/v polyethyleneimine. Radioactive counts were assayed in a γ-counter (Wallac 1261 Multigamma) for [^{125}I]αBTX binding and by a scintillation counter (Beckman LS 6500) for [^{3}H]MLA binding.

Metabolic labelling and immunoprecipitation

To facilitate immunoprecipitation, an eight amino acid FLAG epitope tag (DYKDDDDK) was introduced at the extreme C terminus of the α4, α5 and α6 chimaeric constructs by site-directed mutagenesis, using the QuikChange mutagenesis system (Stratagene). Transfected tsA201 cells were metabolically labelled as described previously (Cooper and Millar, 1997). After growth in methionine-free medium for 15 min, cells were labelled with 9–12 MBq Pro-mix, a mixture of [^{35}S]methionine and [^{35}S]cysteine, (GE Healthcare) in 3.5 ml methionine-free medium for 3 h. Complete medium containing 10% heat-inactivated FCS was then added and the cells incubated for a further 90 min. Cells were washed twice with 6 ml phosphate-buffered saline and harvested into 500 μl ice-cold lysis buffer (150 mM NaCl, 50 mM Tris/Cl, pH 8.0, 5 mM EDTA and 1% Triton X-100) containing protease inhibitors (0.25 mM phenylmethylsulphonyl fluoride, 1 mM *N*-ethylmaleimide and 2 μg ml^{-1}, each, of leupeptin, aprotinin and pepstatin). Solubilization and all subsequent steps were performed at 4 °C. The cell lysate was pre-cleared by incubation overnight with 35 μl protein G-sepharose (GE Healthcare) in a 1:1 mixture with lysis buffer. Non-solubilized material was pelleted by centrifugation at 16 000 × *g* for 15 min. Cell lysates were incubated with primary antibody for 3 h. The antibody–receptor complex was immunoprecipitated by the addition of 30 μl protein G-sepharose, incubated for a further 3 h and isolated by centrifugation. Samples were washed four times with 1 ml lysis buffer. Samples were examined by SDS-PAGE (sodium dodecyl sulphate-polyacrylamide gel electrophoresis) followed by autoradiography as described previously (Lansdell *et al*., 1997).

Intracellular calcium assay

Transfected cells were re-plated onto poly-L-lysine-coated black-walled 96-well plates (Marathon Laboratories, London, UK) 18–20 h after transfection. Approximately 24 h after plating, medium was removed and the cells incubated in 50 μl of 1 μM Fluo-4 acetoxymethyl ester (Invitrogen-Molecular Probes, Paisley, UK) in HBSS with 0.02% Pluronic F-127 (Invitrogen-Molecular Probes) for 45–60 min at room temperature. Cells were rinsed twice in HBSS and assayed using a Fluorometric imaging plate reader (FLIPR) (Molecular Devices, Wokingham, UK) in HBSS supplemented with 18.8 mM $CaCl_2$, 8.8 mM sucrose and 6.3 mM HEPES (4-(2-hydroxyethyl)-1-piperazineethanesulfonic acid). Cells were excited at 488 nm and the emitted fluorescence passed through a 510–570 nm band-pass interference filter before detection with a cooled CCD (charge-coupled device) camera. Drug dilutions were prepared in a separate 96-well plate delivered via an automated 96-tip pipettor. Fluorescence measurements were recorded simultaneously for all 96 wells at 1 s intervals, for 120 s, with agonist additions after 25 s. Average fluorescence intensity readings before agonist applications were subtracted.

Electrophysiology

Cells, grown on glass coverslips coated in collagen and polylysine (both 10 μg ml^{-1}), were co-transfected with pEGFP-C2 (Clontech, Mountain View, CA, USA), encoding enhanced green fluorescent protein and plasmids containing

chimaeric nAChR/5-HT_3R subunit cDNA in the ratio of 1:10. Whole-cell recordings were performed at room temperature, 24–72 h after transfection using cells that were identified as expressing green fluorescent protein by fluorescence microscopy. Recording solution contained (in mM) as follows: 110 NaCl, 5.4 KCl, 0.8 $MgCl_2$, 1.8 $CaCl_2$, 25 glucose, 0.9 NaH_2PO_4, 44 $NaHCO_3$. Borosilicate electrodes (GC150F-7.5; Harvard Apparatus, Edenbridge, UK) of resistance 4–8 MΩ contained (in mM) 140 CsCl, 10 HEPES, 10 EGTA (ethylene glycol bis(β-aminoethyl ether)-*N*,*N*,*N*′,*N*′,-tetraacetic acid), 0.5 $CaCl_2$, 29.53 CsOH, pH adjusted to 7.26. The holding potential was −60 mV. Fast cell superfusion was achieved with a θ-barrelled application pipette made from 1.5 mm diameter θ-tubing (AH-30-0114; Harvard Apparatus), which was moved laterally using a stepper motor. A 20-s application of 50 μM DMPP (1,1-dimethyl-4-phenylpiperazinium iodide) was applied and evoked currents recorded using an Axopatch 200B amplifier. These were digitized online at 10 kHz using WinEDR (Strathclyde Electrophysiology Software; www.strath.ac.uk/Departments/PhysPharm) after filtering and further amplification to provide a low-gain 0 Hz–2 kHz record that was used to measure the agonist-induced mean current. The kinetics of desensitization were analysed on 20 s agonist applications. Responses were inverted and fitted with a single exponential or the sum of two exponential functions. A high-gain band-pass (2 Hz–2 kHz Butterworth filter) recording was used for variance and spectral density analysis. The recording was divided into segments of 0.82 s duration and edited to remove any segments with obvious artefacts. A 10% cosine taper window was applied to each segment and the single-sided spectral density computed by fast Fourier transform and averaged over 96 logarithmically spread frequency ranges. The mean background spectrum was subtracted from the mean spectrum in the presence of the agonist to give the net agonist-induced noise spectrum. The single-channel conductance was calculated from the variance of the noise and from integration of the net power spectrum fitted with a single or the sum of two Lorentzian components as appropriate (Dempster, 2001).

Statistics

For multiple comparisons, ANOVA was used with Tukey–Kramer post-test for unequal sample sizes (Prism; GraphPad Software Inc., San Diego, CA, USA).

Results

A series of 14 subunit chimaeras was constructed, each containing the intracellular (M3–M4) loop domain from a different nAChR subunit (α1–α10 and β1–β4). All chimaeras contained a common extracellular domain (from the nAChR α7 subunit) and the four transmembrane domains from the 5-HT_{3A} subunit (Figure 1a). Previous studies have shown that a similar chimaera ($\alpha7^{V201-5HT3A}$), which contains the intracellular loop domain of the 5-HT_{3A} subunit, generates functional homopentameric receptors with a high-affinity binding site for [^{125}I]αBTX (Eiselé *et al*., 1993; Cooper and Millar, 1998). As $\alpha7^{V201-5HT3A}$ and the loop chimaeras examined in this study contain an α7 extracellular domain and 5-HT_{3A} transmembrane domains, they might be expected to bind [^{125}I]αBTX unless subunit folding or assembly was disrupted by changes in the intracellular loop region.

Loop chimaeras were expressed in the human cultured cell line tsA201 by transient transfection. Intact cells were examined by cell-surface [^{125}I]αBTX binding, which revealed significant differences in the level of specific binding with different loop chimaeras (Figure 1b). The highest levels of cell-surface [^{125}I]αBTX binding were detected with chimaeras containing the α1, α4, α7 and α8 loop domains (~1400–1800 fmol per mg protein). Intermediate levels of cell-surface [^{125}I]αBTX binding (~500–750 fmol per mg protein) were detected with chimaeras containing the α3 and α6 loop domains (Figure 1b). In contrast, specific cell-surface binding of [^{125}I]αBTX was low or absent with chimaeras containing α2, α5, α9, α10, β1, β2, β3 and β4 loop domains (Figure 1b). Levels of [^{125}I]αBTX binding to loop chimaeras are summarized in Table 1.

To examine whether differences in levels of radioligand binding could be attributed to differences in levels of subunit expression, levels of subunit protein were examined by introduction of a recombinant epitope tag to facilitate detection by immunoprecipitation. The α4, α5 and α6 loop constructs were selected (as examples of constructs displaying high, low and intermediate levels of cell-surface [^{125}I]αBTX binding, respectively). A recombinant FLAG epitope tag was introduced at the C terminus. FLAG-tagged subunit chimaeras were expressed in tsA201 cells and metabolically labelled (with [^{35}S]methionine and [^{35}S]cysteine). Tagged subunits were immunoprecipitated with mAbFLAG-M2 and examined by SDS-PAGE, followed by autoradiography. Bands of the expected molecular weight were detected for all three subunit chimaeras and were of a similar intensity (Figure 2). If anything, the chimaera showing the lowest level of cell-surface [^{125}I]αBTX binding (the α5 loop chimaera; Figure 1b) gave a somewhat more intense band on SDS-PAGE (Figure 2). This would suggest that differences in the levels of cell-surface [^{125}I]αBTX binding for these chimaeras are not a consequence of differences in the levels of expressed subunit protein.

Further radioligand binding studies were performed with disrupted cell preparations to determine levels of total (that is, both surface and internal) binding sites. To reduce levels of nonspecific binding, binding studies with disrupted cells were performed with [^{3}H]MLA, rather than [^{125}I]αBTX. For all loop chimaeras, specific binding of [^{3}H]MLA was detected, although differences in the level of binding were observed. (Figure 1c).

To examine whether the loop chimaeras are able to generate functional ligand-gated ion channels, subunit chimaeras were expressed in tsA201 cells and examined using a FILPR, an approach which has been shown previously to be well suited to the functional screening of nAChR/5-HT_3R subunit chimaeras (Gee *et al*., 2007). Evidence of functional ion channel expression (assayed by agonist-induced elevations in intracellular calcium) was observed with chimaeras containing the α3, α7, α8 and α10 loop domains (data not shown). Interestingly, despite the high levels of cell-surface radioligand binding detected, no

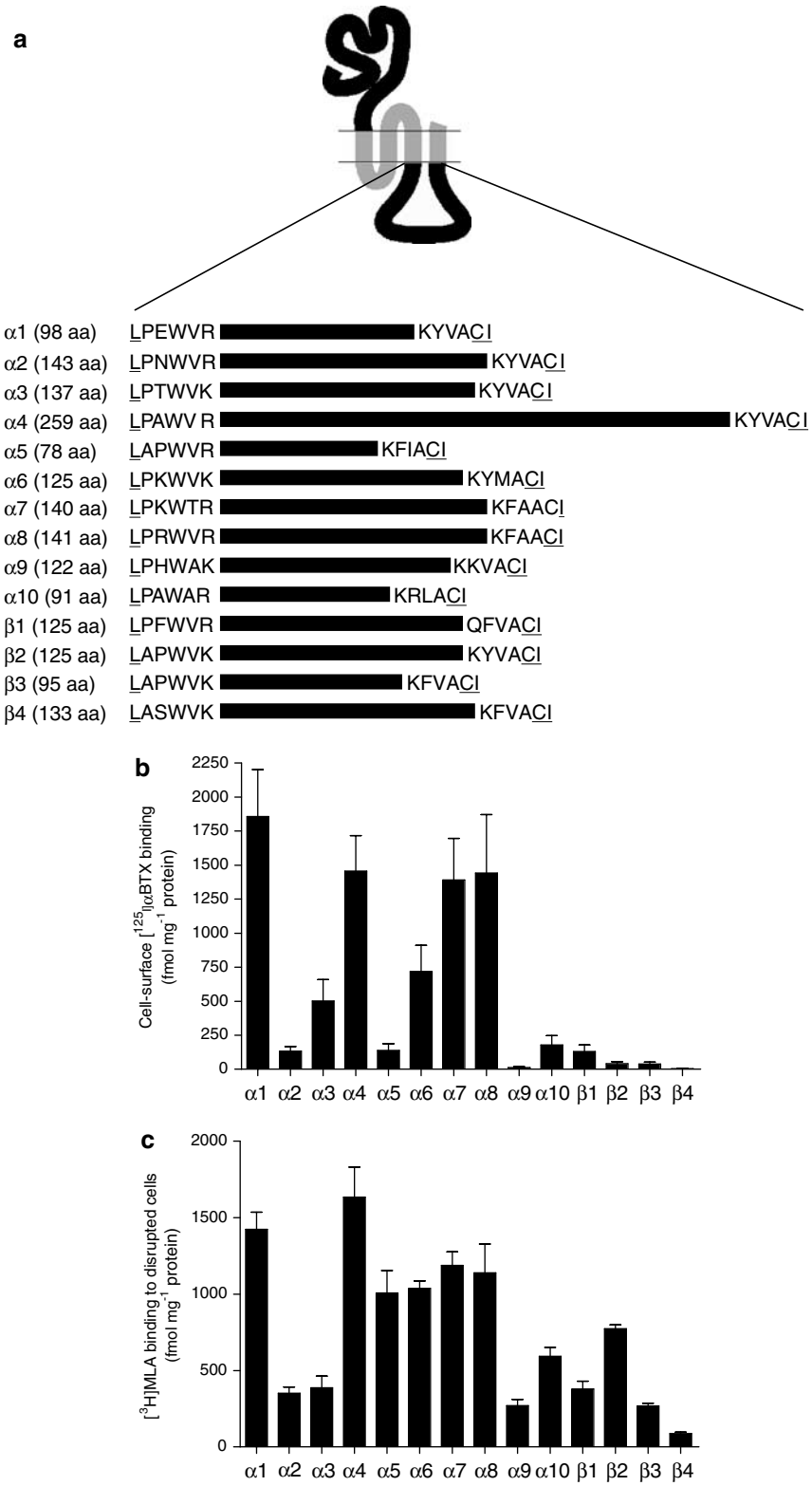

Figure 1 Intracellular (M3–M4 loop) chimaeras. (**a**) A series of subunit chimaeras was constructed containing the intracellular M3–M4 loop domain from all vertebrate nAChR α and β subunits (α1–α10 and β1–β4). All subunit chimaeras contained a common extracellular domain (from the nAChR α7 subunit) and common transmembrane domains (from the 5-HT_{3A} subunit). Horizontal lines represent the approximate relative length of the various intracellular loop domains of each subunit. The exact number of amino acids (aa) within each of these subunit domains is indicated next to the subunit name. To illustrate more clearly the location of the loop domains examined, the six N- and C-terminal amino acids of each domain are indicated. Amino acids that were altered by the introduction of *Not*I and *Bst*Z17I restriction enzyme sites are underlined. (**b**) Cell-surface [^{125}I]αBTX binding to loop chimaeras expressed in human tsA201 cells. (**c**) Binding of [^{3}H]MLA to loop chimaeras determined with disrupted tsA201 cells. Data in (**b** and **c**) are presented as fmol per mg protein and are means of 3–7 independent experiments, each performed in triplicate. Error bars represent s.e.mean. αBTX, α-bungarotoxin; MLA, methyllycaconitine.

Table 1 Characterization of nAChR/5-HT_3R subunit chimaeras

Loop chimaera	*[^{125}I]αBTX binding (fmol mg^{-1}) (n = 4–7)*	*[^{3}H]MLA binding (fmol mg^{-1}) (n = 5)*	*Functional expression*	*Conductance (pS) (n = 5–9)*	*Time constant for desensitization (ms) (n = 6–21)*	*Targeting (MDCK cells)*
α1 loop (α7/5-$HT_{3A}^{\alpha1\text{-loop}}$)	1857 ± 346[a]	1424 ± 111[c]	No	ND	ND	Non-polarized
α2 loop (α7/5-$HT_{3A}^{\alpha2\text{-loop}}$)	132 ± 34[b]	353 ± 39[d]	No	ND	ND	ND
α3 loop (α7/5-$HT_{3A}^{\alpha3\text{-loop}}$)	502 ± 158	388 ± 75[d]	Yes	29.4 ± 2.8[e]	278 ± 23[g]	ND
α4 loop (α7/5-$HT_{3A}^{\alpha4\text{-loop}}$)	1457 ± 259[a]	1635 ± 197[c]	No	ND	ND	Apical
α5 loop (α7/5-$HT_{3A}^{\alpha5\text{-loop}}$)	139 ± 48[b]	1008 ± 148[c]	No	ND	ND	ND
α6 loop (α7/5-$HT_{3A}^{\alpha6\text{-loop}}$)	718 ± 193	1037 ± 50[c]	No	ND	ND	ND
α7 loop (α7/5-$HT_{3A}^{\alpha7\text{-loop}}$)	1391 ± 307[a]	1187 ± 89[c]	Yes	36.1 ± 3.2[e]	1334 ± 141[h]	Apical
α8 loop (α7/5-$HT_{3A}^{\alpha8\text{-loop}}$)	1442 ± 429[a]	1139 ± 189[c]	Yes	24.9 ± 0.8[e]	967 ± 184[h]	Apical
α9 loop (α7/5-$HT_{3A}^{\alpha9\text{-loop}}$)	13 ± 5[b]	272 ± 41[d]	No	ND	ND	ND
α10 loop (α7/5-$HT_{3A}^{\alpha10\text{-loop}}$)	179 ± 69[b]	592 ± 60	Yes	10.5 ± 1.7[f]	217 ± 16[g]	ND
β1 loop (α7/5-$HT_{3A}^{\beta1\text{-loop}}$)	129 ± 48[b]	381 ± 50[d]	No	ND	ND	ND
β2 loop (α7/5-$HT_{3A}^{\beta2\text{-loop}}$)	41 ± 16[b]	775 ± 24	No	ND	ND	ND
β3 loop (α7/5-$HT_{3A}^{\beta3\text{-loop}}$)	40 ± 12[b]	269 ± 18[d]	No	ND	ND	ND
β4 loop (α7/5-$HT_{3A}^{\beta4\text{-loop}}$)	5 ± 2[b]	88 ± 10[d]	No	ND	ND	ND

Abbreviations: αBTX, α-bungarotoxin; MDCK, Madin–Darby canine kidney; MLA, methyllycaconitine; ND, not determined.
Data shown are means ± s.e.mean.
Statistical significance: [a] vs [b] $P<0.05$, [c] vs [d] $P<0.05$, [e] vs [f] $P<0.001$, [g] vs [h] $P<0.001$.

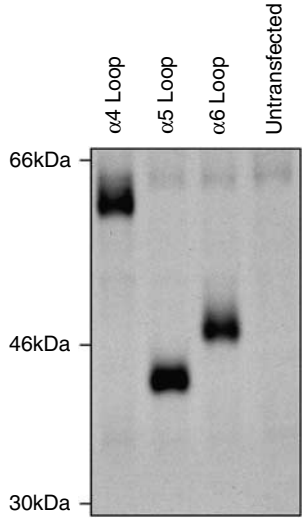

Figure 2 Immunoprecipitation of FLAG-tagged loop chimaeras. An FLAG epitope tag was introduced at the C terminus of chimaeras containing intracellular loop domains from the α4, α5 and α6 subunits. Tagged chimaeras were immunoprecipitated from metabolically labelled human tsA201 cells and examined by SDS-PAGE. The α4, α5 and α6 loop chimaeras are representative of chimaeras displaying high, low and intermediate levels of [^{125}I]αBTX, respectively, but expressed levels of subunit protein appear to be broadly similar. The positions of molecular weight markers are shown. αBTX, α-bungarotoxin; SDS-PAGE, sodium dodecyl sulphate-polyacrylamide gel electrophoresis.

evidence of functional expression was observed with the α1 or α4 loop constructs.

As previous studies have demonstrated that, among receptors in the Cys-loop superfamily, the M3–M4 intracellular loop domain can exert a dramatic influence upon single-channel conductance (Kelley *et al*., 2003; Hales *et al*., 2006; Gee *et al*., 2007), we have determined the single-channel conductance of receptors generated by the loop chimaeras. Previous studies conducted with $\alpha7^{V201-5HT3A}$ (which contains a 5-HT_{3A} intracellular loop) identified a single-channel conductance of 0.8 ± 0.1 pS, $n = 5$ (Gee *et al*., 2007), which is not significantly different from the sub-pS conductance observed with the wild-type 5-HT_{3A} subunit (0.7 ± 0.1 pS, $n = 5$) recorded under identical conditions (Gee *et al*., 2007). As a control for the present studies on the nAChR loop chimaeras, we have independently determined the conductance of the $\alpha7^{V201-5HT3A}$ chimaera. A conductance estimate of 0.5 ± 0.1 pS ($n = 5$) was obtained, which is not significantly different from that reported previously (Gee *et al*., 2007).

Previous studies have reported that a subunit chimaera containing the α7 intracellular loop ($\alpha7^{4TM-5HT3A}$) generates receptors with a single-channel conductance of 30.5 ± 4.0 pS, which is significantly larger ($P<0.001$) than the sub-pS conductance of both 5-HT_{3A} and of the $\alpha7^{V201-5HT3A}$ chimaera (Gee *et al*., 2007). We have performed noise analysis of whole-cell responses to determine the single-channel conductance of chimaeras containing the α3, α7, α8 and α10 loop domains. As the α7 loop chimaera (α7/5-$HT_{3A}^{\alpha7\text{-loop}}$) is essentially equivalent to the previously described $\alpha7^{4TM-5HT3A}$ chimaera (Gee *et al*., 2007), it would be expected to give similar results. The α7 loop chimaera does, however, contain two amino acid differences from the previously described $\alpha7^{4TM-5HT3A}$ chimaera (methionine to leucine and valine to isoleucine mutations, which arose due to introduction of the *Not*I and *Bst*Z17I sites into $\alpha7^{4TM-5HT3A}$; see Materials and methods for details). The single-channel conductance determined in this study for the α7 loop chimaera (Table 1) was not significantly different to that determined previously by Gee *et al*. (2007) for the $\alpha7^{4TM-5HT3A}$ chimaera (see above).

All the nAChR loop chimaeras examined (α3, α7, α8 and α10 loop domains) generated receptors with single-channel conductances, which were significantly larger ($P<0.001$) than the sub-pS conductance observed with the 5-HT_{3A} loop domain (Figure 3). Significant differences were also observed between chimaeras containing different nAChR subunit loop

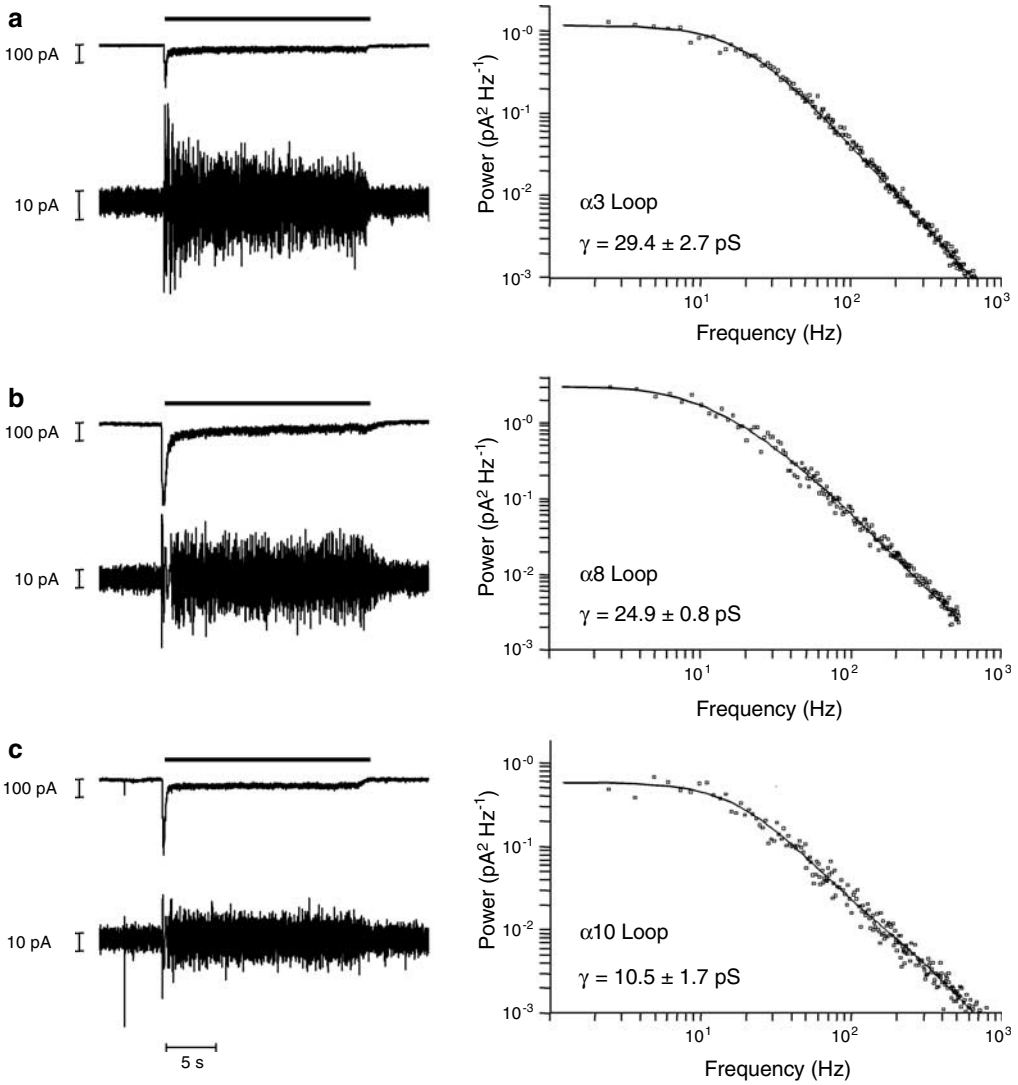

Figure 3 Influence of nAChR subunit loop domains upon single-channel conductance. Chimaeric subunits containing the M3–M4 intracellular loop domain from the α3 subunit (**a**), α8 subunit (**b**) or α10 subunit (**c**) were expressed in tsA201 cells and analysed by whole-cell recording. Representative whole-cell responses were obtained by a 20-s application (thick horizontal scale bar) of 50 μM DMPP (left panel). Vertical scale bars = 100 pA. Below each whole-cell response is shown a high-gain band-pass filtered (2 Hz–2 kHz) record illustrating the increase in noise variance associated with each response. Vertical scale bars = 10 pA. Representative plots illustrating the noise power spectrum (right panel) for each chimaera are also shown. Estimates of channel conductance were derived from both noise spectral analysis and plots of variance against mean current of 5–9 cells. Conductance estimates are presented here as a mean from both types of analysis with standard errors. DMPP, 1,1-dimethyl-4-phenylpiperazinium iodide; nAChR, nicotinic acetylcholine receptor.

domains. Chimaeras with the highest conductance were those that contained the α3, α7 and α8 loop (Table 1). The α10 loop chimaera gave an intermediate conductance, which was both significantly smaller than that observed with the α3, α7 and α8 loop chimaeras (Table 1; $P<0.001$) and significantly larger than that observed with the 5-HT_{3A} loop chimaera ($P<0.001$).

The influence of the intracellular loop upon desensitization was also examined. All chimaeras tested showed extensive desensitization (see Figure 4), but significant differences were detected in the time constant for desensitization for different loop chimaeras (Figure 4 and Table 1). The decay time constants for chimaeras containing the α7 and α8 loop domains were significantly larger ($P<0.001$; $n=8$–21) than those determined with chimaeras containing the α3 and α10 loop domains (Table 1).

Finally, the influence of intracellular loop domains upon receptor targeting was examined by expression of loop chimaeras in polarized epithelial MDCK cells. Fluorescence confocal microscopy was used to detect the distribution of subunit chimaeras labelled with Alexa-488 αBTX (Figures 5a and c). For comparison, staining of endogenous E-cadherin, which is expressed exclusively on basolateral membranes (Mays *et al*., 1995), was examined (Figures 5b and c). Subunits that displayed high levels of specific [^{125}I]αBTX binding (α1, α4, α7 and α8 loop chimaeras) were expressed in polarized MDCK cells. Fluorescence confocal microscopy revealed predominantly apical staining for chimaeras

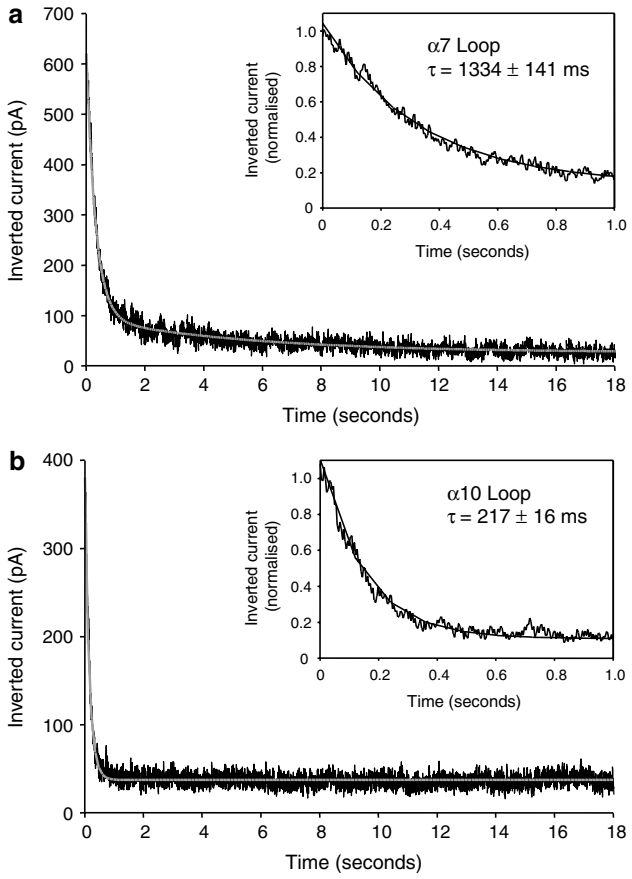

Figure 4 Influence of nAChR intracellular domain upon the kinetics of desensitization. α7 loop (**a**) and α10 loop (**b**) are shown as examples of chimaeras with slow and fast desensitization, respectively. Subunits chimaeras were expressed in tsA201 cells whole-cell responses obtained by 20 s applications of 50 μM DMPP. These were inverted and fitted with one or the sum of two exponential functions of the form $I = I_{ss} + I_{max} * e^{(-t/\tau)}$, where I_{ss} is the steady state current, I_{max} the peak steady-state current, τ, the time constant. The insets show, on an expanded timescale, the fit to the initial part of the response. Traces are representative examples of $n = 8$–21 responses from 3–12 cells. DMPP, 1,1-dimethyl-4-phenylpiperazinium iodide; nAChR, nicotinic acetylcholine receptor.

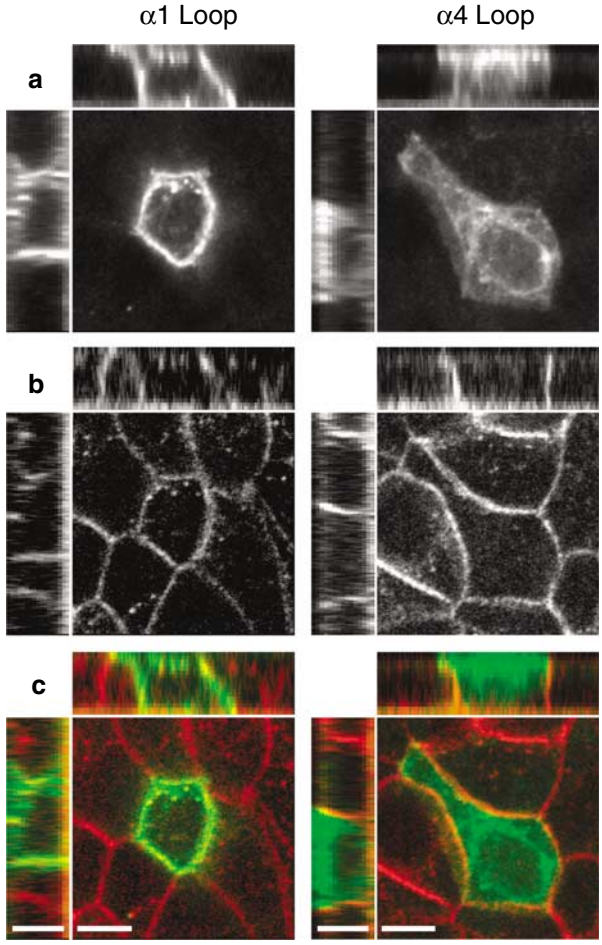

Figure 5 Targeting of loop chimaeras examined in polarized epithelial (MDCK) cells. Representative confocal images are shown illustrating a non-polarized distribution of the α1 loop chimaera (left panels) and a polarized (apical) distribution of the α4 loop chimaera (right panels). The main images are single confocal section from 15–17 separate 0.5 μm sections. Above and to the left of the main images are representative *X–Z* and *Y–Z* confocal sections from each image in which the apical cell surface is located at the top and to the left, respectively. (**a**) Labelling of subunit chimaeras with Alexa-488 αBTX. (**b**) Antibody (rhodamine) staining of endogenous E-cadherin, which is located on the basolateral membrane of MDCK cells. (**c**) Merged images from (**a** and **b**) in which Alexa-488 αBTX staining is shown in green and antibody staining of endogenous E-cadherin is shown in red. Scale bars = 7 μm. αBTX, α-bungarotoxin; MDCK, Madin–Darby canine kidney.

containing the α4, α7 and α8 loop domains. In contrast, the α1 loop chimaera displayed a non-polarized (apical and basolateral) distribution (Figures 5a and c).

Discussion

A series of subunit chimaeras has been constructed with the aim of investigating the influence of nAChR and 5-HT_3 receptor intracellular domains upon phenomena such as receptor assembly, cell-surface expression, intracellular targeting and function. All chimaeras contained a common extracellular domain (derived from the nAChR α7 subunit) and common transmembrane regions (from the 5-HT_{3A} subunit). As has been demonstrated previously, these features facilitate both detection of expressed subunit chimaeras by αBTX and efficient homomeric assembly (Eiselé *et al*., 1993; Cooper and Millar, 1998; Gee *et al*., 2007). Consequently, all of the loop chimaeras examined in this study would be expected to bind [^{125}I]αBTX, unless subunit folding or assembly was disrupted by the intracellular loop domain. Interestingly, we have observed substantial differences in the levels of cell-surface [^{125}I]αBTX binding with different loop chimaeras (Figure 1b). These differences appear not to be a consequence of differences in the level of expressed subunit protein, as loop chimaeras with high, low and intermediate levels of cell-surface [^{125}I]αBTX binding were detected in similar amounts by immunoprecipitation of the FLAG-tagged chimaeras (Figure 2).

All chimaeras were also examined using radioligand binding on disrupted cells, thereby permitting detection of

intracellular, as well as cell-surface, receptors. Whereas some loop chimaeras could not be detected on the cell surface, all of the intracellular loop chimaeras gave detectable levels of specific radioligand binding in disrupted cell preparations (Figure 1c). We assume that differences in the level of [^{3}H]MLA binding reflect differences in the efficiency with which loop chimaeras are able to fold and oligomerize into a native conformation (Figures 1b and c). Comparisons of the two sets of radioligand binding data indicate that intracellular loop domains influence both efficiency of subunit folding/assembly and also the proportion of correctly folded receptors, which are detectable on the cell surface. For example, the α5, α6 and α7 loop chimaeras have similar levels of [^{3}H]MLA binding in disrupted cells (Figure 1c) but very different levels of cell-surface [^{125}I]αBTX binding (Figure 1b).

A FLIPR-based assay was used to assess whether nAChR/5-HT$_3$R chimaeras were able to generate functional receptors (Gee *et al*., 2007). As expected, no evidence of functional expression was detected for loop chimaeras, which failed to give cell-surface [^{125}I]αBTX binding. As has been demonstrated previously for the α7 loop chimaera (Gee *et al*., 2007), clear evidence of functional expression was observed for the α3, α8 and α10 loop chimaeras. Interestingly, a good correlation was not observed between those chimaeras that displayed high levels of cell-surface [^{125}I]αBTX binding and those for which clear evidence of functional expression could be detected. The α1 and α4 loop chimaeras, for example, gave high levels of cell-surface [^{125}I]αBTX binding, but no evidence of functional expression. The α3 and α10 loop chimaeras gave relatively low levels of cell-surface [^{125}I]αBTX binding, but clear evidence of functional expression. It appears, therefore, that the nAChR intracellular loop domain can also exert a profound influence upon the ability of subunits, once assembled, to generate functional receptors. Similar discrepancies between levels of radioligand binding and function have been reported in studies with other types of nAChR subunit chimaeras and with subunits altered by site-directed mutagenesis (García-Guzmán *et al*., 1994; Valor *et al*., 2002; Castelán *et al*., 2007; Gee *et al*., 2007).

Taken together, the radioligand binding and FLIPR data suggest that the M3–M4 loop exerts a strong influence on subunit folding and receptor trafficking. It is interesting, for example, that chimaeras containing the α1 or α4 M3–M4 loops are expressed efficiently on the cell surface, whereas wild-type α1 and α4 subunits, when expressed alone, are not efficient (Green and Claudio, 1993; Cooper *et al*., 1999). This is presumably due to chimaeras containing these loops being able to assemble into pentameric complexes, whereas unassembled subunits such as α1 and α4 are retained within the endoplasmic reticulum (Green and Millar, 1995). It is possible that those chimaeras that were not detected at high levels on the cell surface (for example, those containing α2, α5, α9, α10, β1, β2, β3 and β4 loop domains) contain intracellular retention signals. Such signals may, perhaps, be masked when wild-type subunits assemble into heteromeric complexes, thereby facilitating cell-surface expression, as has been described for other Cys-loop receptor subunits (Boyd *et al*., 2003). The lack of correlation between chimaeras that generated high levels of cell-surface [^{125}I]αBTX binding and those that generated functional channels (Table 1) is also of interest. It is possible that there are critical folding events in which the M3–M4 loop domain participates, which are required for the generation of functional receptors.

Despite the well-established evidence that the conductance of Cys-loop type ligand-gated ion channels is influenced by amino acids located within the second transmembrane domain, there is now strong evidence to indicate that channel conductance is also influenced by other subunit domains, including the M3–M4 intracellular loop (Kelley *et al*., 2003; Hales *et al*., 2006; Gee *et al*., 2007). Noise analysis of the loop chimaeras is entirely consistent with previous data implicating the intracellular loop in modulating channel conductance. It has been proposed that the influence of the intracellular loop domain is a consequence of positively charged amino acids (Kelley *et al*., 2003; Hales *et al*., 2006), and it has been demonstrated that the replacement of three arginine residues within the membrane-associated amphipathic (MA) region of the 5-HT$_{3A}$ subunit intracellular loop results in a dramatic increase in single-channel conductance (Kelley *et al*., 2003). Inspection of the MA region of the subunits examined in this study (α3, α7, α8 and α10) indicates that our findings are in general agreement with the proposal that positively charged amino acids in this region are important.

Our results provide evidence that the rate of receptor desensitization is influenced by the M3–M4 intracellular domain. This is perhaps a surprising finding, given that residues within the M2 transmembrane domain of nAChRs have been shown to be important in determining rates of receptor desensitization (Revah *et al*., 1991). There is, however, evidence that subunit domains other than M2 can influence desensitization. Recent studies with nAChR/5-HT$_3$R subunit chimaeras have demonstrated that the N-terminal extracellular domain can influence receptor desensitization (Gee *et al*., 2007). Taken together, these results indicate that receptor desensitization can be influenced by a variety of subunit domains.

The ability of intracellular loop domains to influence receptor targeting has been examined in polarized epithelial MDCK cells. MDCK cells have been used extensively to examine the targeting of transmembrane proteins (Mellman, 1995; Nelson and Yeaman, 2001) and have also been used to demonstrate the influence of subunit composition upon the targeting of GABA$_A$ receptors (Connolly *et al*., 1996). Cultured MDCK cells establish clearly defined and easily identifiable polarized membranes. As a control, we examined the distribution of endogenous E-cadherin, a protein which is selectively targeted to the basolateral membrane in MDCK cells (Mays *et al*., 1995). As the selective targeting of E-cadherin to the basolateral membrane is dependent on MDCK polarization (van Beest *et al*., 2006), this also provides a means of confirming cells are polarized. MDCK cells are well suited for studies with αBTX, as they do not express endogenous nAChRs. In addition, there is evidence to indicate that sorting of transmembrane proteins to epithelial apical and basolateral membranes is a useful model for axonal and dendritic sorting in neurons (de Hoop and Dotti, 1993). A clear difference was observed between the muscle

nAChR α1 loop chimaera (which displayed a non-polarized distribution) and neuronal nAChR α4, α7 and α8 loop chimaeras (which displayed apical targeting). These loop chimaeras have provided a useful mechanism by which to examine independently the role of intracellular domains of individual nAChR subunits. The use of these chimaeras has also circumvented difficulties we have encountered in detecting efficient expression of neuronal nAChR subunit combinations in MDCK cells. These studies suggest that nAChR targeting is influenced by the M3–M4 intracellular loop domain, a conclusion which is in agreement with previous studies in chick ciliary ganglion neurons (Williams *et al*., 1998). Furthermore, these studies demonstrate that in these constructs, the nAChR M3–M4 intracellular domain contains determinants of receptor targeting, which can function in the absence of neuron-specific interacting proteins.

In summary, we have constructed a series of subunit chimaeras that have enabled the influence of intracellular domains of nAChR subunits to be examined independently of other co-assembled subunits. There is evidence that demonstrates that the intracellular (M3–M4) domain exerts an important influence upon subunit folding and assembly (as demonstrated by radioligand binding) and upon the formation of functional receptors. It is also clear that the intracellular domain influences both the efficiency of cell-surface expression and the targeting of assembled subunits in polarized cells. Evidence to support the involvement of the nAChR intracellular domain in determining single-channel conductance has also been obtained.

Acknowledgements

This work was supported by grants from the Wellcome Trust. SK was supported by a Wellcome Trust PhD studentship.

Conflict of interest

The authors state no conflict of interest.

References

Alexander SPH, Mathie A, Peters JA (2007). Guide to receptors and channels (GRAC), 2nd edition (2007 revision). *Br J Pharmacol* **150** (Suppl 1): S1–S168.

Boyd GW, Doward AI, Kirness EF, Millar NS, Connolly CN (2003). Cell surface expression of 5-hydroxytryptamine type 3 receptors is controlled by an endoplasmic reticulum retention signal. *J Biol Chem* **278**: 27681–27687.

Castelán F, Mulet J, Aldea M, Sala S, Sala F, Criado M (2007). Cytoplasmic regions adjacent to the M3 and M4 transmembrane segments influence expression and function of α7 nicotinic acetylcholine receptors. A study with single amino acid mutants. *J Neurochem* **100**: 406–415.

Connolly CN, Wooltorton JRA, Smart TG, Moss SJ (1996). Subcellular localization of γ-aminobutyric acid type A receptors is determined by receptor β subunits. *Proc Natl Acad Sci USA* **93**: 9899–9904.

Cooper ST, Harkness PC, Baker ER, Millar NS (1999). Upregulation of cell-surface α4β2 neuronal nicotinic receptors by lower temperature and expression of chimeric subunits. *J Biol Chem* **274**: 27145–27152.

Cooper ST, Millar NS (1997). Host cell-specific folding and assembly of the neuronal nicotinic acetylcholine receptor α7 subunit. *J Neurochem* **68**: 2140–2151.

Cooper ST, Millar NS (1998). Host cell-specific folding of the neuronal nicotinic receptor α8 subunit. *J Neurochem* **70**: 2585–2593.

Couturier S, Bertrand D, Matter JM, Hernandez MC, Bertrand S, Millar N *et al*. (1990). A neuronal nicotinic acetylcholine receptor subunit (α7) is developmentally regulated and forms a homo-oligomeric channel blocked by α-BTX. *Neuron* **5**: 847–856.

de Hoop MJ, Dotti CG (1993). Membrane traffic in polarized neurons in culture. *J Cell Sci Suppl* **17**: 85–92.

Dempster J (2001). *The Laboratory Computer: A Practical Guide for Physiologists and Neuroscientists*. Academic Press: London.

Eiselé J-L, Bertrand S, Galzi J-L, Devillers-Thiéry A, Changeux J-P, Bertrand D (1993). Chimaeric nicotinic-serotonergic receptor combines distinct ligand binding and channel specificities. *Nature* **366**: 479–483.

Elgoyhen AB, Johnson DS, Boulter J, Vetter DE, Heinemann S (1994). α9: an acetylcholine receptor with novel pharmacological properties expressed in rat cochlear hair cells. *Cell* **18**: 705–715.

Elgoyhen AB, Vetter DE, Katz E, Rothlin CV, Heineman SF, Boulter J (2001). α10: a determinant of nicotinic cholinergic receptor function in mammalian vestibular and cochlear mechanosensory hair cells. *Proc Natl Acad Sci USA* **98**: 3501–3506.

García-Guzmán M, Sala F, Sala S, Campos-Caro A, Criado M (1994). Role of two acetylcholine receptor subunit domains in homomer formation and intersubunit recognition, as revealed by α3 and α7 subunit chimeras. *Biochemistry* **33**: 15198–15203.

Gee VJ, Kracun S, Cooper ST, Gibb AJ, Millar NS (2007). Identification of domains influencing assembly and ion channel properties in α7 nicotinic receptor and 5-HT_3 receptor subunit chimaeras. *Br J Pharmacol* **152**: 501–512.

Gerzanich V, Anand R, Lindstrom J (1994). Homomers of α8 and α7 subunits of nicotinic receptors exhibit similar channels but contrasting binding site properties. *Mol Pharmacol* **45**: 212–220.

Gotti C, Hanke W, Maury K, Moretti M, Ballivet M, Clementi F *et al*. (1994). Pharmacology and biophysical properties of α7 and α7–α8 α-bungarotoxin receptor subtypes immunopurified from the chick optic lobe. *Eur J Neurosci* **6**: 1281–1291.

Green WN, Claudio T (1993). Acetylcholine receptor assembly: subunit folding and oligomerization occur sequentially. *Cell* **74**: 57–69.

Green WN, Millar NS (1995). Ion-channel assembly. *Trends Neurosci* **18**: 280–287.

Hales TG, Dunlop JI, Deeb TZ, Carland JE, Kelley SP, Lambert JJ *et al*. (2006). Common determinants of single channel conductance within the large cytoplasmic loop of 5-hydroxytryptamine type 3 and α4β2 nicotinic acetylcholine receptors. *J Biol Chem* **281**: 8062–8071.

Huebsch KA, Maimone MM (2003). Rapsyn-mediated clustering of acetylcholine receptor subunits requires the major cytoplasmic loop of the receptor subunits. *J Neurobiol* **54**: 484–501.

Jeanclos EM, Lin L, Treuil MW, Rao J, DeCoster MA, Anand R (2001). The chaperone protein 14-3-3η interacts with the nicotinic acetylcholine receptor α4 subunit. *J Biol Chem* **276**: 28281–28290.

Kassner PD, Berg DK (1997). Differences in the fate of neuronal acetylcholine receptor protein expressed in neurons and stably transfected cells. *J Neurobiol* **33**: 968–982.

Kelley SP, Dunlop JI, Kirkness EF, Lambert JJ, Peters JA (2003). A cytoplasmic region determines single-channel conductance in 5-HT_3 receptors. *Nature* **424**: 321–324.

Keyser KT, Britto LR, Schoepfer R, Whiting P, Cooper J, Conroy W *et al*. (1993). Three subtypes of α-bungarotoxin-sensitive nicotinic acetylcholine receptors are expressed in chick retina. *J Neurosci* **13**: 442–454.

Lansdell SJ, Schmitt B, Betz H, Sattelle DB, Millar NS (1997). Temperature-sensitive expression of *Drosophila* neuronal nicotinic acetylcholine receptors. *J Neurochem* **68**: 1812–1819.

Le Novère N, Changeux J-P (1995). Molecular evolution of the nicotinic acetylcholine receptor: an example of multigene family in excitable cells. *Mol Evol* **40**: 155–172.

Lester HA, Dibas MI, Dahan DS, Leite JF, Dougherty DA (2004). Cys-loop receptors: new twists and turns. *Trends Neurosci* **27**: 329–336.

Mays RW, Siemers KA, Fritz BA, Lowe AW, van Meer G, Nelson WJ (1995). Hierarchy of mechanisms involved in generating Na/K-ATPase polarity in MDCK epithelial cells. *J Cell Biol* **130**: 1105–1115.

Mellman I (1995). Molecular sorting of membrane proteins in polarized and nonpolarized cells. *Cold Spring Harb Symp Quant Biol* **60**: 745–752.

Millar NS (2003). Assembly and subunit diversity of nicotinic acetylcholine receptors. *Biochem Soc Trans* **31**: 869–874.

Millar NS (2006). Ligand-gated ion channels. In: *Encyclopedia of Life Sciences*. John Wiley and Sons Ltd: Chichester, http://www.els.net/ [doi:10.1038/npg.els.0000154].

Nelson WJ, Yeaman C (2001). Protein trafficking in the exocytic pathway of polarized epithelial cells. *Trends Cell Biol* **11**: 483–486.

Rangwala F, Drisdel RC, Rakhilin S, Ko E, Atluri P, Harkins AB *et al*. (1997). Neuronal α-bungarotoxin receptors differ structurally from other nicotinic acetylcholine receptors. *J Neurosci* **17**: 8201–8212.

Revah F, Bertrand D, Galzi JL, Devillers-Thiery A, Mulle C, Hussy N *et al*. (1991). Mutations in the channel domain alter desensitization of a neuronal nicotinic receptor. *Nature* **353**: 846–849.

Séguéla P, Wadiche J, Dineley-Miller K, Dani JA, Patrick JW (1993). Molecular cloning, functional properties, and distribution of rat brain α7: a nicotinic cation channel highly permeable to calcium. *J Neurosci* **13**: 596–604.

Valor LM, Mulet J, Sala F, Ballesta JJ, Criado M (2002). Role of the large cytoplasmic loop of the α7 neuronal nicotinic acetylcholine receptor subunit in the receptor expression and function. *Biochemistry* **41**: 7931–7938.

van Beest M, Robben JH, Savelkoul PJM, Hendriks G, Devonald MAJ, Konings IBM *et al*. (2006). Polarisation, key to good localisation. *Biochim Biophys Acta* **1758**: 1126–1133.

Williams BM, Temburni MK, Levey MS, Bertrand S, Bertrand D, Jacob MH (1998). The long internal loop of the α3 subunit targets nAChRs to subdomains within individual synapses on neurones *in vivo*. *Nat Neurosci* **1**: 557–562.